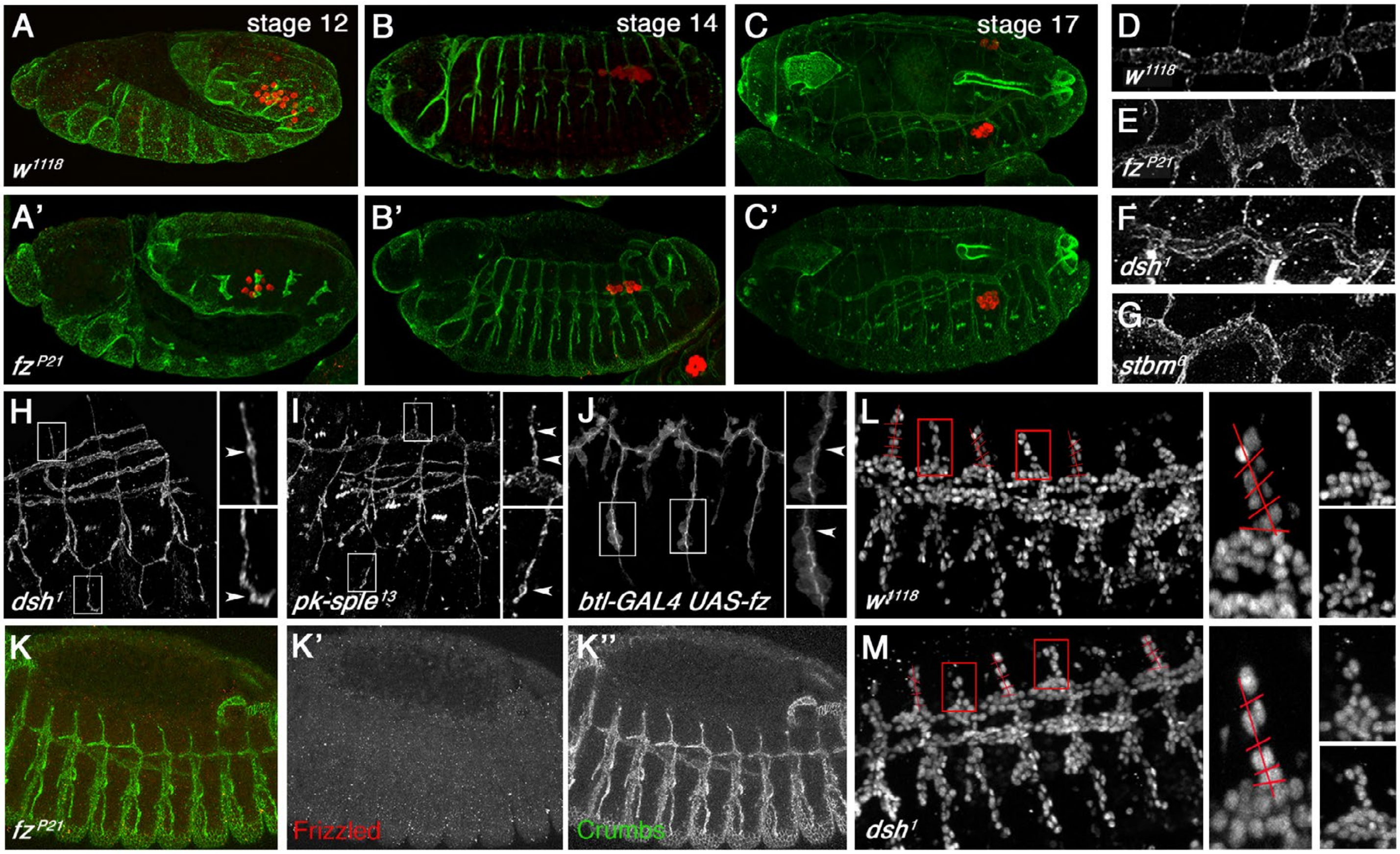

Fig. S1. Effects of loss of core planar polarity activity on embryonic and tracheal system development. (**A-C′**) Scoring stage of tracheal development versus general embryonic development on the basis of embryonic morphology (epidermal tissues stained with anti-Crumbs in green) and pole cell migration (stained for anti-Vasa in red) shows no delay in tracheal development in embryos lacking core pathway activity. w^{1118} (wild type) (A-C) and fz^{P21} (A′-C′) embryos at stage 12 (A,A′), stage 14 (B,B′) and stage 17 (C,C′). (**D-G**) Dorsal trunk labelled with Crumbs in w^{1118} (wild type) (D), and planar polarity mutants fz^{P21} (E), dsh^1 (F), $stbm^6$ (G). (**H-J**) Lateral view of embryonic tracheal branches at stage 14 showing defects in cell intercalation in core pathway mutant embryos stained for the junctional marker Crumbs in dsh^1 (H) and $pk\text{-}sple^{13}$ (I), or GFP in *btl-GAL4/UAS-fz* embryos co-expressing *α-Cat-GFP* (J). Compare with w^{1118} (wild type) in Fig. 1A. Insets show magnified regions of indicated dorsal and ventral branches, arrowheads indicate unresolved intercalations. (**K-K″**) Specificity of the anti-Fz antibody in the embryo. Loss of Fz immunostaining in fz^{P21} mutants [Fz (red or white), Crumbs (green or white)]. Compare with supplementary material Fig.S2D. (**L**,**M**) Tracheal cells are similarly aligned in stage 13 dorsal branches in wild-type (L) and dsh^1 (M) embryos. The larger insets show examples of well-aligned pairs of cells and smaller insets show poorly aligned pairs of cells (marked as red boxes on main panel), in both genotypes.

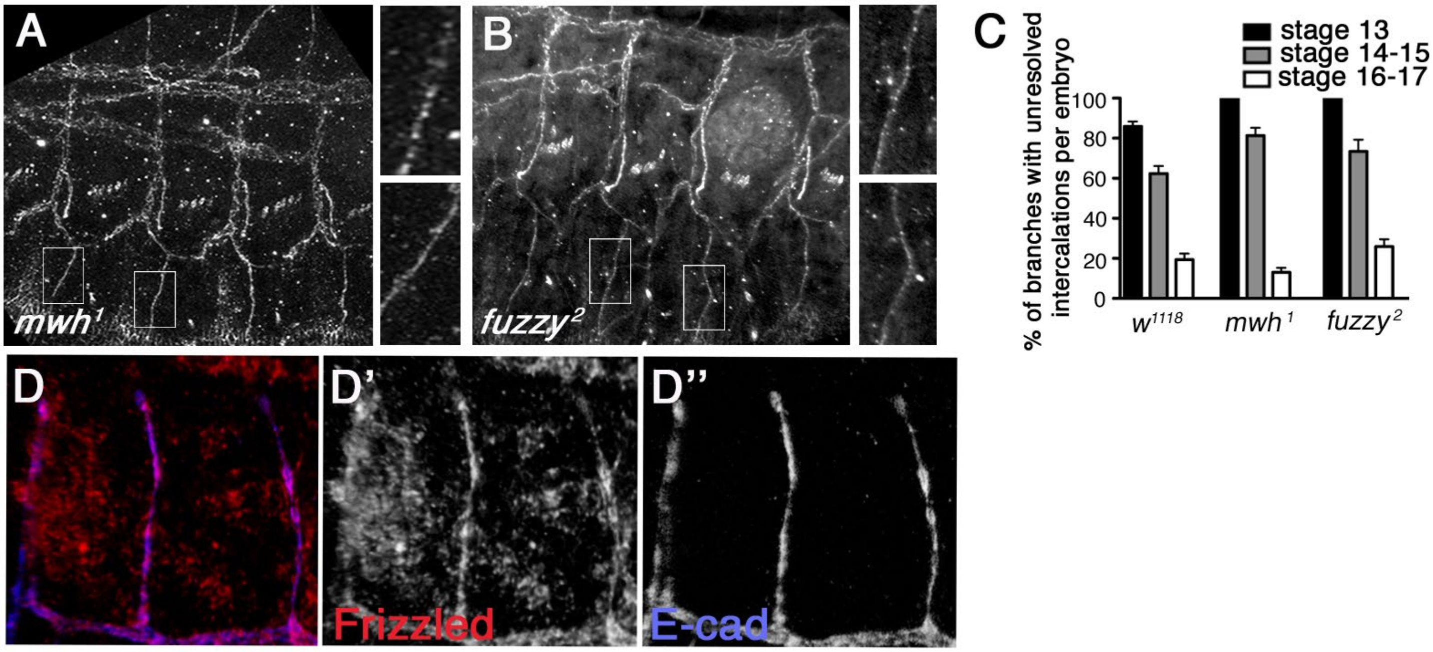

Fig. S2. Fuzzy and Multiple Wing Hairs are not required for tracheal branch intercalation. (**A**,**B**) Lateral view of embryonic tracheal branches at stage 14 showing cell intercalation in embryos lacking activity of downstream effectors of the core pathway, stained for the junctional marker Crumbs. (A) *mwh¹* (B) *fuzzy²*. Compare with *w¹¹¹⁸* (wild type) in Fig. 1A. Insets show magnified regions of indicated branches. (**C**) Quantification of the number of branches with unresolved intercalations at stages 13, 14-15 and 16-17. Error bars are s.e.m. ANOVAs were used to compare the wild-type control and the mutant conditions at each stage: stage 13, P=0.012; stage 14-15, P=0.072; stage 16-17, P=0.069. (**D**) Co-labelling of Fz (red in D or white in D′) and E-cad (blue in D or white in D″) in junctions of stage 15 tracheal branches.

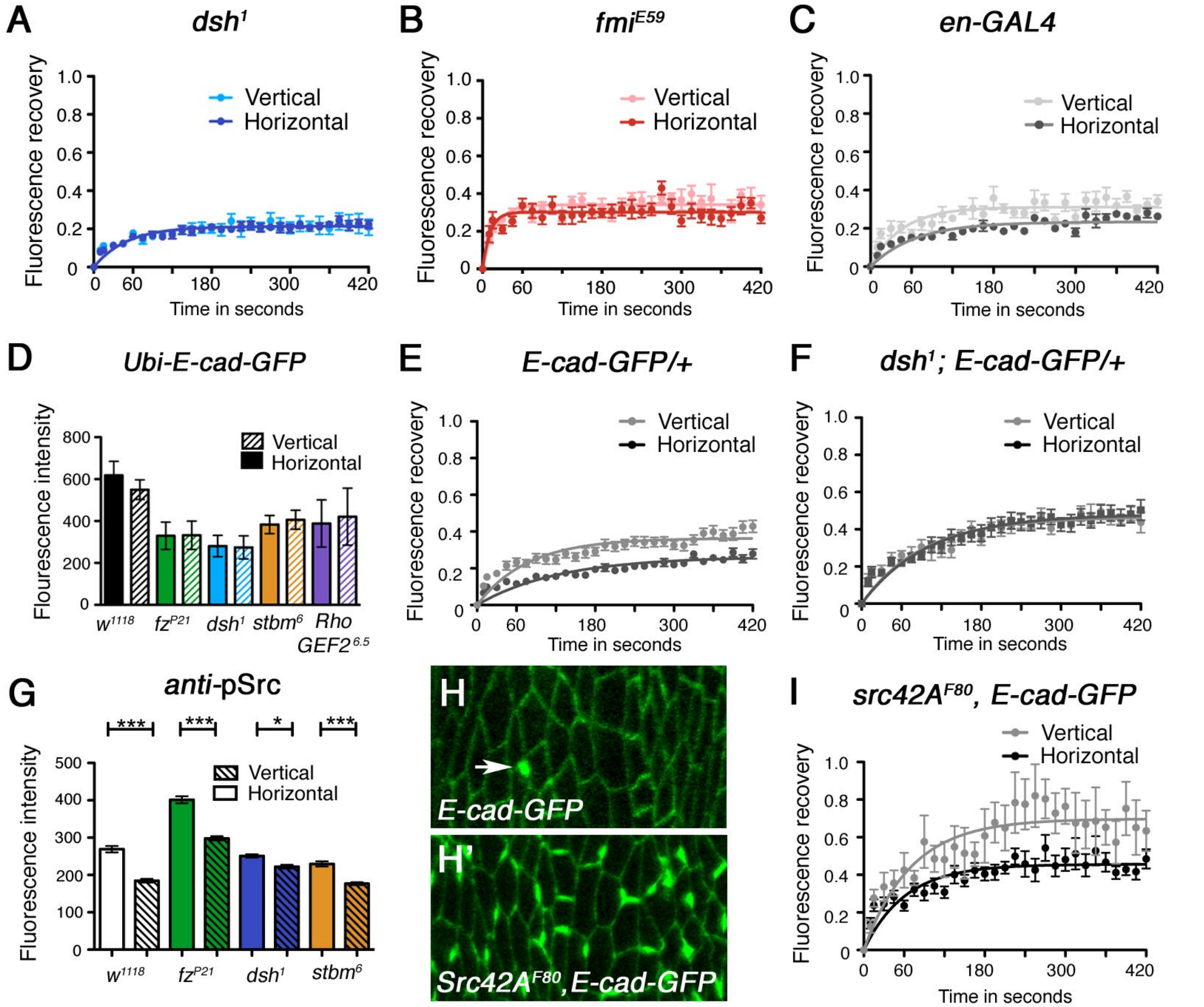

Fig. S3. Effects of the core planar polarity pathway and Src42A on E-cad turnover in the embryonic epidermis. (**A-C**) FRAP analysis in the epidermis of junctional E-cad-GFP expressed under control of the *ubiquitin* promoter in dsh^1 embryos (P=0.83 comparing stable fractions on vertical and horizontal junctions, t-test), fmi^{E59} (P=0.13), *en-GAL4* ($P\leq0.0001$). (**D**) Quantification of E-cad-GFP under control of the *ubiquitin* promoter in the epidermis at stage 8, measured on vertical and horizontal junctions, for w^{1118} (wild type) (black bars), and core pathway mutants fz^{P21} (green bars), dsh^1 (blue bars), $stbm^6$ (orange bars) and $RhoGEF2^{6.5}$/+ antimorphs (purple bars). Note that E-cad is no longer enriched on horizontal junctions in the mutant backgrounds, but overall E-cad-GFP levels go down, presumably due to competition from increased levels of endogenous E-cad. (**E**,**F**) FRAP analysis of junctional E-cad-GFP expressed under its endogenous promoter, one copy of E-cad-GFP present heterozygous with one copy of wild-type E-cad. In a wild-type background, a larger stable fraction is seen on horizontal junctions than on vertical junctions ($P\leq0.0001$, t-test); this difference is lost in a dsh^1 background (P=0.63, t-test). (**G**) Quantification of pSrc on horizontal and vertical junctions in the epidermis of stage 8 embryos, w^{1118} (wild type) (white bars) and core pathway mutants fz^{P21} (green bars), dsh^1 (blue bars) and $stbm^6$ (orange bars). pSrc remains higher on horizontal than vertical junctions in the absence of core protein activity; however, overall levels are increased in a similar fashion to the increase in overall E-cad levels seen in these backgrounds (compare with Fig. 4G). pSrc asymmetry is therefore independent of either core protein activity or E-cad distribution; however, additional E-cad at junctions may be recruiting additional Src, consistent with the reported physical interaction between Src and E-cad (Takahashi et al., 2005). An ANOVA comparing all intensities shows that they vary significantly, $P\leq0.0001$. Asterisks above chart show individual results from the ANOVA. *P=0.0123, ***P<0.0001. (**H**) Localisation of E-cad-GFP expressed at endogenous levels in a wild-type background (H) and in a *Src42A* zygotic mutant (H′). E-cad-GFP localises to the junctions in the *Src42A* background, and large aggregates of E-cad-GFP are also visible localising at the cell periphery. Arrow indicates a sensory organ precursor. (**I**) FRAP analysis was performed on regions of the junctions away from the large aggregates of E-cad-GFP. E-cad-GFP recovery still shows a difference between vertical and horizontal junctions in *Src42A* mutant embryos ($P\leq0.0001$, t-test).

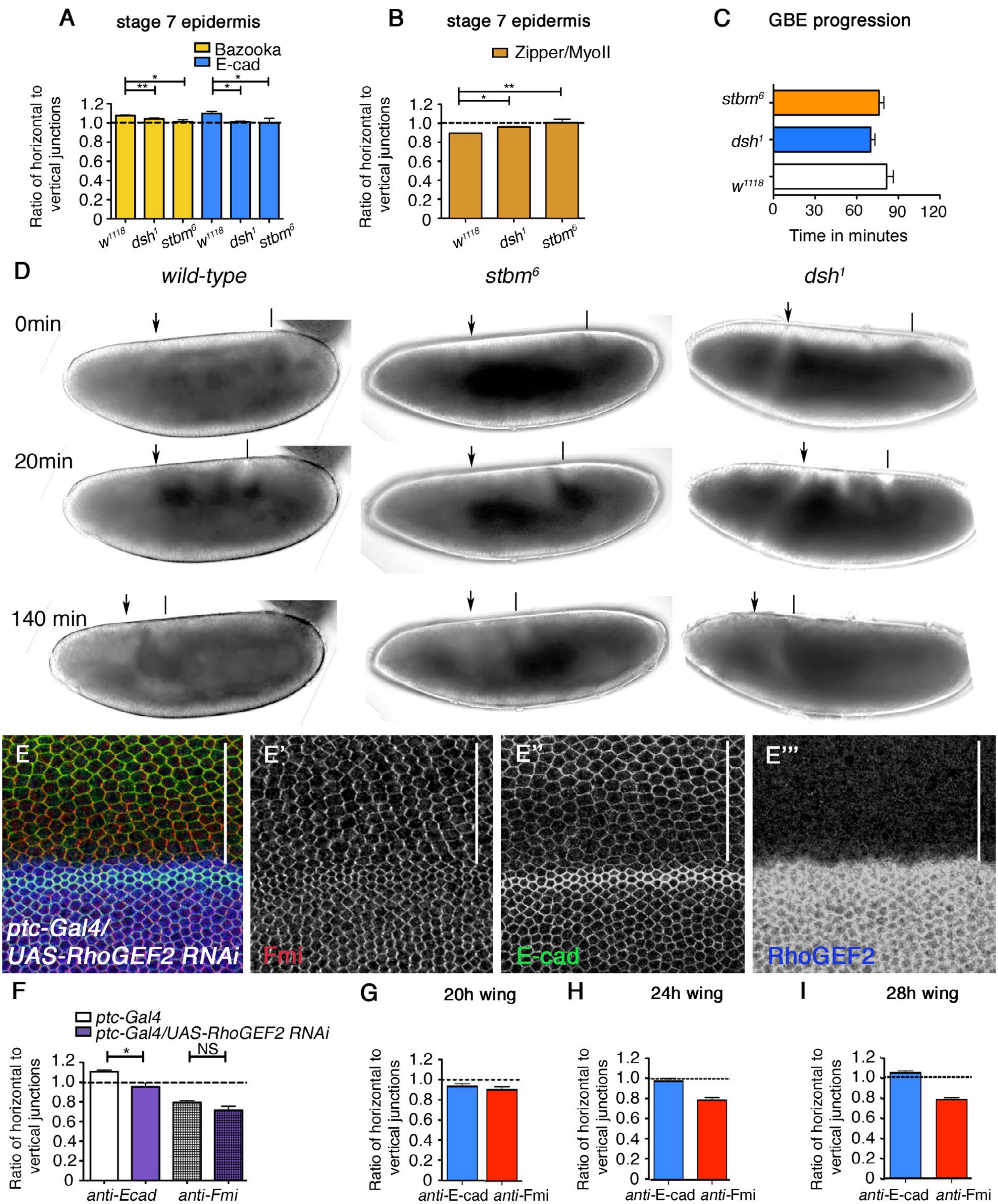

A
stage 7 epidermis
Bazooka
E-cad
Ratio of horizontal to vertical junctions
w1118
dsh1
stbm6
B
stage 7 epidermis
Zipper/MyoII
C
GBE progression
Time in minutes
D
wild-type
stbm6
dsh1
0min
20min
140 min
E
E'
E''
E'''
ptc-Gal4/
UAS-RhoGEF2 RNAi
Fmi
E-cad
RhoGEF2
F
ptc-Gal4
ptc-Gal4/UAS-RhoGEF2 RNAi
NS
anti-Ecad
anti-Fmi
G
20h wing
H
24h wing
I
28h wing
anti-E-cad
anti-Fmi

Fig. S4. Effects of core pathway mutants on protein asymmetry and germband extension in the embryo. (**A**) Quantification of Bazooka (yellow) and E-cad (blue) asymmetric localisation on horizontal and vertical junctions in stage 7 ventrolateral epidermis in wild type (*w^{1118}*), *dsh^1* and *$stbm^6$* shown as ratio of horizontal to vertical (a value of 1 indicates symmetric localisation). Asterisks above the charts show individual results from a Dunnett's multiple comparison test (*$P\leq0.05$, **$P\leq0.01$). (**B**) Quantification of Zipper on horizontal and vertical junctions in stage 7 epidermis in wild type (*w^{1118}*), *dsh^1* and *$stbm^6$*. *P=0.0114, **P=0.0009. (**C**) Quantification of the time taken for the fast phase of germband elongation to complete for wild type (*w^{1118}*) and *dsh^1* and *$stbm^6$* mutants; an ANOVA test shows that *w^{1118}* is not significantly different from the mutants (P=0.3411). (**D**) Images of germband extending wild-type (*w^{1118}*), *dsh^1* and *$stbm^6$* embryos at 0 minutes, 20 minutes and 140 minutes. Arrows indicate the anterior furrow, lines indicate the posterior end of the germband. (**E-E‴**) RhoGEF2 knockdown by RNAi in the *ptc-GAL4* domain of a pupal wing (indicated by white line) immunolabelled for RhoGEF2 (blue in E, white in E‴), Fmi (red in E, white in E′) and E-cad (green in E, white in E"). Wild-type tissue is in the lower part of the image. E‴ shows RhoGEF2 antibody specificity, loss of RhoGEF2 staining in *ptc-Gal4/UAS-RhoGEF2 RNAi* region. (**F**) Quantification of intensity ratios comparing horizontal with vertical junctions. E-cad (plain bars) and Fmi (checked bars) levels were compared in the *ptc-GAL4* domain of wings expressing *ptc-Gal4/UAS-RhoGEF2-RNAi* (purple bars) and control *ptc-GAL4* domains in wings expressing only *ptc-Gal4* (white bars). Asterisks above the charts show individual results from *t*-tests (NS, not significant; *$P\leq0.05$). Defects in cell packing were also investigated in the *ptc-GAL4* domain expressing *RhoGEF2-RNAi* compared with control *ptc-GAL4* wings (see Materials and methods); however, no difference was observed (*ptc-GAL4/UAS-RhoGEF2-RNAi*, mean number of cell sides=5.762 seconds, s.d.=0.754; *ptc-GAL4* only, mean number of cell sides=5.831 second, s.d.=0.671; *t*-test, P=0.0655). (**G-I**) Quantification of endogenous junctional E-cad (blue) and Fmi (red) asymmetry in pupal wings showing ratios of anterior-posterior junctions to proximal-distal junctions at 20 hours (J), 24 hours (K) and 28 hours (L). Error bars are s.d.

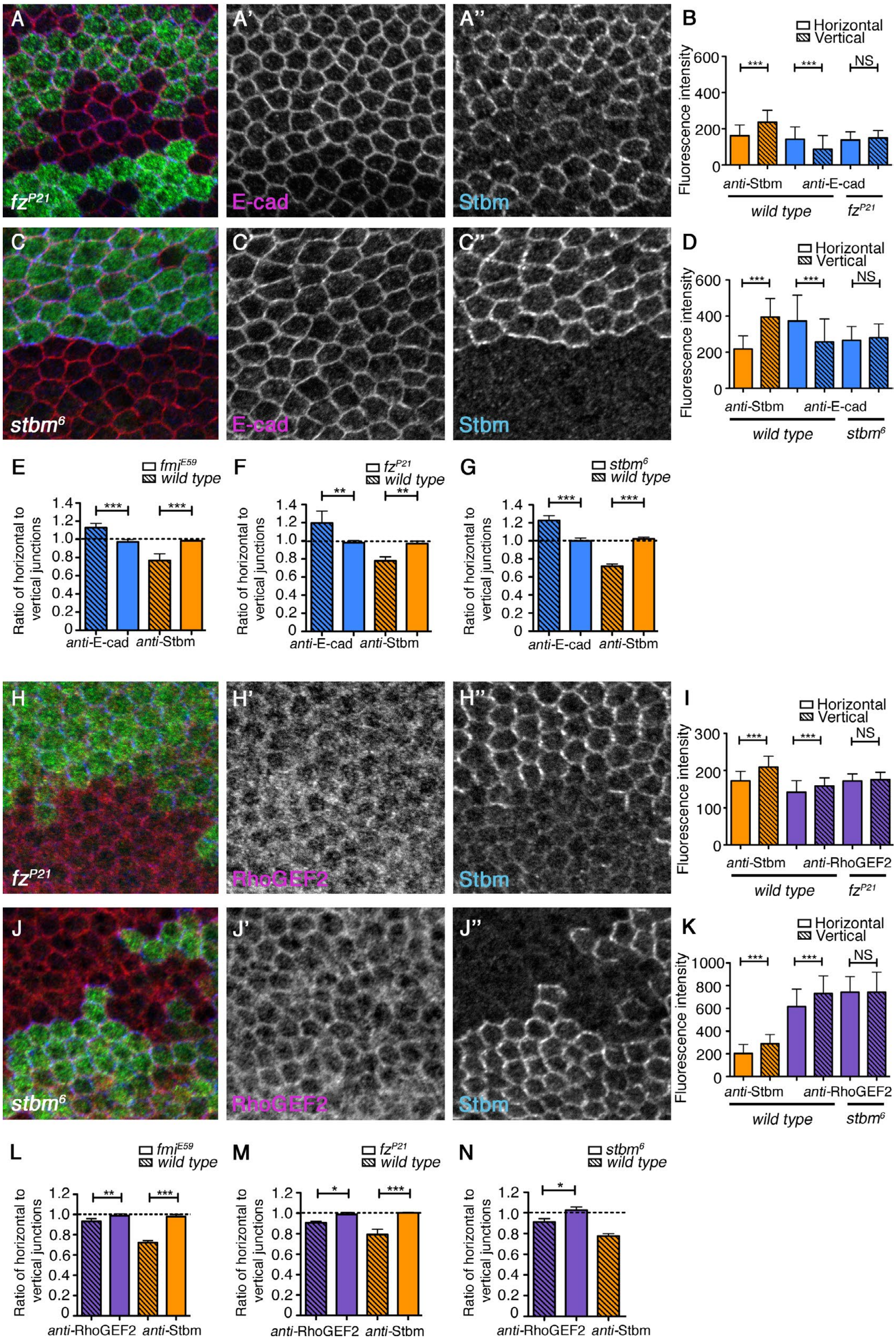

A
fz^P21
A'
E-cad
A''
Stbm
B
Horizontal
Vertical
Fluorescence intensity
anti-Stbm
anti-E-cad
wild type
fz^P21
NS
C
stbm^6
C'
E-cad
C''
Stbm
D
Horizontal
Vertical
Fluorescence intensity
anti-Stbm
anti-E-cad
wild type
stbm^6
NS
E
fmi^E59
wild type
Ratio of horizontal to vertical junctions
anti-E-cad
anti-Stbm
F
fz^P21
wild type
Ratio of horizontal to vertical junctions
anti-E-cad
anti-Stbm
G
stbm^6
wild type
Ratio of horizontal to vertical junctions
anti-E-cad
anti-Stbm
H
fz^P21
H'
RhoGEF2
H''
Stbm
I
Horizontal
Vertical
Fluorescence intensity
anti-Stbm
anti-RhoGEF2
wild type
fz^P21
NS
J
stbm^6
J'
RhoGEF2
J''
Stbm
K
Horizontal
Vertical
Fluorescence intensity
anti-Stbm
anti-RhoGEF2
wild type
stbm^6
NS
L
fmi^E59
wild type
Ratio of horizontal to vertical junctions
anti-RhoGEF2
anti-Stbm
M
fz^P21
wild type
Ratio of horizontal to vertical junctions
anti-RhoGEF2
anti-Stbm
N
stbm^6
wild type
Ratio of horizontal to vertical junctions
anti-RhoGEF2
anti-Stbm

Fig. S5. Effects of the core pathway on E-cad and RhoGEF2 localisation in the 28 hour pupal wing. (**A-A″**) E-cad (magenta in A, white in A′) and Stbm (blue in A, white in A″) in a fz^{P21} pupal wing clone marked by absence of *lacZ* expression (green in A). Distal is to the right in these and the following images. (**B**) Quantification of endogenous junctional E-cad in wild type and fz^{P21} (blue bars), and Stbm (orange bars) in wild-type 28 hour pupal wings. E-cad is increased on the horizontal junctions in wild-type tissue but this is lost in fz^{P21} (*t*-tests comparing horizontal and vertical intensities: Stbm in wild type, $P \leq 0.0001$; E-cad in wild type, $P \leq 0.0001$; E-cad in fz^{P21}, P=0.0770). All error bars in this figure are s.d. (**C-C″**) Endogenous E-cad (magenta in C, white in C′) and Stbm (blue in C, white in C″) in a $stbm^6$ pupal wing clone marked by absence of *lacZ* expression (green in C). (**D**) Quantification of endogenous junctional E-cad in wild type and $stbm^6$ (blue bars), and Stbm (orange bars) in wild-type 28 hour pupal wings. E-cad is increased on the horizontal junctions in wild-type tissue but this is lost in $stbm^6$ (*t*-tests comparing horizontal and vertical intensities: Stbm in wild type, $P \leq 0.0001$; E-cad in wild type, $P \leq 0.0001$; E-cad in $stbm^6$, P=0.1279). (**E-G**) Ratios of E-cad and Stbm on horizontal and vertical junctions in wild-type and fmi^{E59} (E), fz^{P21} (F) and $stbm^6$ (G). Asterisks above the charts show individual results from a Bonferroni's multiple comparison test (*$P \leq 0.05$, **$P \leq 0.01$, ***$P \leq 0.0001$). (**H-H″**) RhoGEF2 (magenta in H, white in H′) and Stbm (blue in H, white in H″) in a fz^{P21} pupal wing clone marked by absence of *lacZ* expression (green in H). (**I**) Quantification of endogenous junctional RhoGEF2 in wild type and fz^{P21} (purple bars), and Stbm (orange bars) in wild-type 28 hour pupal wings. RhoGEF2 is increased on the vertical junctions in wild-type tissue but this is lost in fz^{P21} (*t*-tests comparing horizontal and vertical intensities: Stbm in wild type, $P \leq 0.0001$; RhoGEF2 in wild type, $P \leq 0.0001$; RhoGEF2 in fz^{P21}, P=0.2030). (**J-J″**) RhoGEF2 (magenta in J, white in J′) and Stbm (blue in J, white in J″) in a $stbm^6$ pupal wing clone marked by absence of *lacZ* expression (green in J). (**K**) Quantification of endogenous junctional RhoGEF2 in wild type and $stbm^6$ (purple bars), and Stbm (orange bars) in wild-type 28 hour pupal wings. RhoGEF2 is increased on the vertical junctions in wild-type tissue but this is lost in $stbm^6$ (*t*-tests comparing horizontal and vertical intensities: Stbm in wild type, $P \leq 0.0001$; RhoGEF2 in wild type, $P \leq 0.0001$; RhoGEF2 in $stbm^6$, P=0.9960). (**L-N**) Ratios of RhoGEF2 and Stbm on horizontal and vertical junctional in wild type and fmi^{E59} (L), fz^{P21} (M) and $stbm^6$ (N). Asterisks above the charts show individual results from a Bonferroni's multiple comparison test (*$P \leq 0.05$, **$P \leq 0.01$, **$P \leq 0.0001$).

Table S1. List of mutant alleles and transgenic constructs used

Name of gene	Allele	Class	Comments	Flybase reference
white	w^{1118} (outcrossed to Oregon R)	n/a	Used as wild type	FBgn0003996
frizzled	fz^{P21}	Null allele	Crossed out to wild type	FBal0004937
strabismus (Van Gogh)	$stbm^{6}$	Null allele	Crossed out to wild type	FBal0062423
dishevelled	dsh^{1}	Strong allele for planar polarity function	Crossed out to wild type	FBal0003138
prickle-spiny-legs	$pk\text{-}sple^{13}$	Null allele	Crossed out to wild type	FBal0060943
flamingo (*starry night*)	fmi^{E59}	Null allele		FBal0101421
multiple wing hairs	mwh^{1}	Null allele	Crossed out to wild type	FBal0012675
fuzzy	$fuzzy^{2}$	Null allele	Crossed out to wild type	FBal0004916
RhoGEF2	$RhoGEF2^{6.5}$	Antimorphic allele	Zygotic mutants die early	FBal0085926
shotgun	shg^{IG27}	P-element loss of function allele		FBgn0003391
Src42A	$Src42A^{F80}$	Amino acid substitution in the kinase domain		FBal0277626

Name of construct	Comments	Flybase reference
UAS-fz	UAS-driven expression of *frizzled*	FBal0060399
$en\text{-}Gal4^{e16E}$	Gal4 driven by the *engrailed* promoter	FBal0052377
shg-lacZ	*lacZ* enhancer trap insertion in the *shotgun* (*E-cadherin*) locus	FBtp0039292
btl-Gal4	Gal4 expression by the *breathless* promoter	FBti0072919
$UAS\text{-}Apoliner^{5}$	UAS-driven expression of Apoliner on II	FBti0131165
UAS-red-stinger	UAS-driven expression of red stinger-NLS on III	FBtp0018199
UAS-α-Cat-GFP	UAS-driven expression of α-Catenin tagged with GFP	FBti0015823
$UAS\text{-}Rab5^{SN}$	UAS-driven expression of Rab5 dominant negative	FBal0189754
$UAS\text{-}shg\text{-}DEFL^{6.3}$ *(GFP),*	UAS-driven expression of E-cadherin tagged with GFP	FBti0015825
$UAS\text{-}RhoGEF2^{5}$	UAS-driven expression of RhoGEF2	FBal0190772
$RhoGEF2^{IR\text{-}HMS01118}$	UAS-driven expression of RNAi targeting RhoGEF2	FBtp0065361
$UAS\text{-}RhoA^{V14}$	UAS-driven expression of $RhoA^{V14}$ dominant active	FBal0105124
$UAS\text{-}RhoA^{N19}$	UAS-driven expression of $RhoA^{N19}$ dominant negative	FBtp0008154
dsh-GFP	Dishevelled tagged with GFP expressed under its endogenous promoter	FBti0017855
Ubi-E-cad-GFP	E-cadherin tagged with GFP expressed under control of the *ubiquitin* promoter	FBtp0014096
E-cad::GFP	Knock-in of GFP into the endogenous *E-cadherin* (*shotgun*) locus	FBal0247908
hs-FLP	Yeast FLP recombinase under control of a *heat-shock* promoter	FBst0005256
btl>y+>GAL4	*breathless* promoter upstream of the GAL4 coding sequence, separated by an FRT cassette containing a *yellow* transgene	FBtp0020129
ptc-GAL4	Gal4 driven by the *patched* promoter	FBal0040487
UAS-pk	UAS-driven expression of Prickle	FBal0101220